Structural Engineering and Mechanics, Vol. 24, No. 1 (2006) 31-50
DOI: http://dx.doi.org/10.12989/sem.2006.24.1.031

Large deformation analysis of inflated air-spring shell made of rubber-textile cord composite

Tran Huu Nam† and Tran Ich Thinh‡

Department of Material and Structure Mechanics, Hanoi University of Technology, Vietnam

(Received December 21, 2005, Accepted April 18, 2006)

Abstract. This paper deals with the mechanical behaviour of the thin-walled cylindrical air-spring shell (CAS) made of rubber-textile cord composite (RCC) subjected to different types of loading. An orthotropic hyperelastic constitutive model is presented which can be applied to numerical simulation for the response of biological soft tissue and of the nonlinear anisotropic hyperelastic material of the CAS used in vibroisolation of driver's seat. The parameters of strain energy function of the constitutive model are fitted to the experimental results by the nonlinear least squares method. The deformation of the inflated CAS is calculated by solving the system of five first-order ordinary differential equations with the material constitutive law and proper boundary conditions. Nonlinear hyperelastic constitutive equations of orthotropic composite material are incorporated into the finite strain analysis by finite element method (FEM). The results for the deformation analysis of the inflated CAS made of RCC are given. Numerical results of principal stretches and deformed profiles of the inflated CAS obtained by numerical deformation analysis are compared with experimental ones.

Keywords: constitutive model; rubber-textile cord composite; air-spring shell.

1. Introduction

Nowadays textile composites and inflatable structures are becoming increasingly popular for a variety of applications in many fields - civil engineering, architecture, vehicle and aerospace engineering. Typical examples include membrane roofs and covers, sails, inflatable buildings and pavillions, airships, inflatable furniture, airspace structures, air-springs etc. The composite materials created of rubber matrix reinforced by textile cords is called *rubber-textile cord composites*. Air-springs form an example of layered multiphase flexible composite structures that consist of rubbery matrix and stiff reinforcement made of textile cords. The high modulus, low elongation cords carry most of the load, and the low modulus, high elongation rubber matrix preserves the integrity of the composite and transfers the load. The primary objective of this type composite is to withstand large deformation and fatigue loading while providing high load carrying capacity.

Recently, classical phenomenological constitutive equations for rubber-like solids, such as Mooney-Rivlin, Neo-Hookean (see Beatty 1987, Holzapfel *et al.* 2000, Bonet and Profit 2000, Guo 2001) or Ogden models (Ogden 2001) are progressively replaced by more physical models based on

† Ph.D., E-mail: thnam-v1@mail.hut.edu.vn
‡ Professor, Ph.D., Corresponding author, E-mail: thinhti@hn.vnn.vn

statistical considerations in various engineering applications. The identification of material parameters of the constitutive models is often performed using classical homogeneous strain experiments (uniaxial extension or pure shear tests for example). For biaxial deformation, Verron and Marckmann (2003) used frequently the bubble inflation technique, that consists in inflating an initially plane circular thin membrane. In this type of experiments, deformations are not homogeneous and the analysis of experimental data needs efficient numerical method to solve the inflation problem.

Motivated mainly by interest in the numerical simulation of hyperelastic materials are some orthotropic and transversely hyperelastic constitutive models have been proposed recently. Most of them are represented by strain energy function formulated as a polynomial (Bonet and Burton 1998) or an exponential (Ogden *et al*. 2000, Holzapfel *et al*. 2000, 2001) or logarithmic function (Poživilová and Plešek 2002) of orthotropic (or transversely isotropic) strain invariants. However, the development of the constitutive theory of anisotropic elastic or viscoelastic materials at finite strains is still far to be complete and the publications in this field are sparse. For the isotropic hyperelastic materials, the Ogden model with a strain energy function formulated in terms of principal stretches has been showed to be advantageous in spite of a relatively complicated numerical realization. This model demonstrates an excellent agreement with experimental results at large strains and involves many other material laws, for example Mooney-Rivlin and Neo-Hookean ones as special case. Therefore, the orthotropic generalization of Ogden model enables to consider various anisotropic hyperelastic materials within a unified concept.

Using FEM to solve the problems of membrane inflation, such as a simplified approach based on the use of Biot stresses in governing equations was proposed by Jiang and Haddow (1995). Their method was successfully applied to the case of initially circular plane membrane. Recently, Shi and Moita (1996) used the finite element (FE) formulation developed previously by Wriggers and Taylor (1990) with the arc-length method to overcome limit points and to calculate secondary branches. Verron and Marckmann (2001) presented network-based hyperelastic constitutive equations in the context of thin membrane inflation and proposed a new B-spline interpolation model for the free inflation of axisymmetric rubber-like membrane. The material models are implemented in a numerical tool that incorporates an efficient B-spline interpolation method and a coupled Newton-Raphson/arc-length solving algorithm. Reese *et al.* (2000, 2001) were developed a model describing the inelastic material behaviour of pneumatic membranes reinforced with roven-woven textile and modeling by finite element for orthotropic material behaviour in pneumatic membranes.

The main purpose of this paper is to identify the parameters of the orthotropic hyperelastic constitutive model and to analysis the large deformation of the inflated CAS made of RCC. The deformation of the inflated CAS is calculated by solving the system of five first-order ordinary differential equations and by FEM. A presented orthotropic constitutive model of RCC is incorporated into the FEM for large deformation analysis of the inflated CAS. The derivation of the axisymmetric shell element kinematics and of the constitutive matrix is presented. The tangent stiffness matrix and the external force vector are also formulated. The computation was carried out in Matlab. Intermediate stages of inflated shell and limit points were computed by the combination of modified Newton-Raphson method with load increments controled by the iteration count of previous convergence and by the arc-length method.

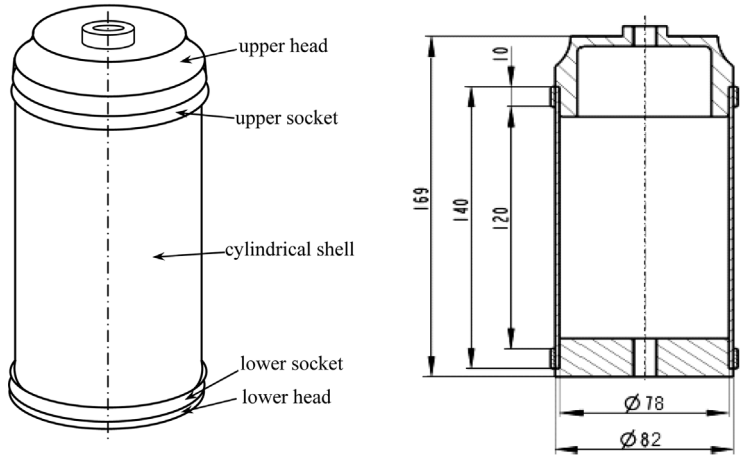

Fig. 1 Cylindrical air-spring shell

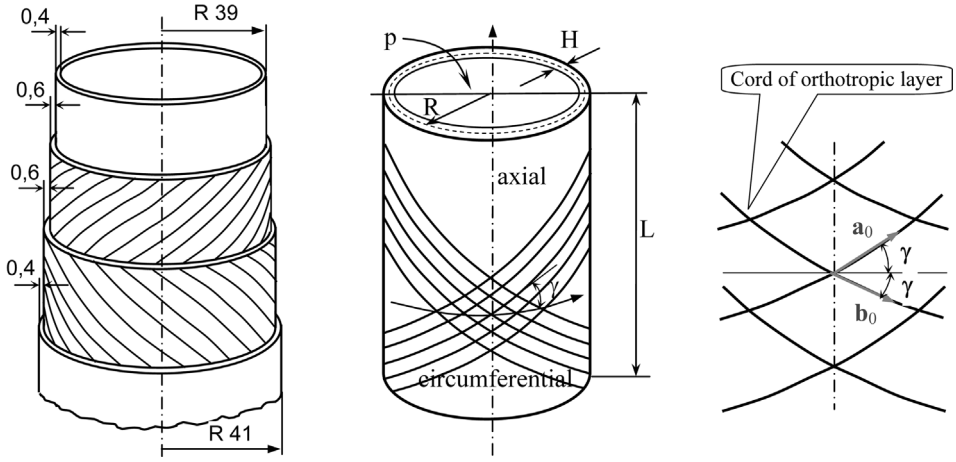

Fig. 2 Textile cord reinforced circular tube of cylindrical air-spring. Continuum model for the structure of the orthotropic layer (with double-helically arranged fibers)

2. Description of structural material and experimental analysis

A CAS (Fig. 1) is usually made up of four layers – the inner and the outer layer of calandered rubber and the two plies of cord reinforced rubber in which the cords have a specific bias angle to the other arranged symmetrically with respect to the circumferential direction (Fig. 2). The resulting material properties are orthotropic in the case of on-axis loading. The cylindrical air-spring is relatively short – the diameter of the tubular shell is $2R = 82$ mm, the height is $L = 120$ mm and the wall thickness is $H = 2$ mm.

The properties of the material and the angle between cords have to be determined experimentally in site since the air-spring is assigned for further experiments and it cannot be dissected for usual material tests. In a 2-D cylindrical polar coordinate system, the components of $\mathbf{a}_0$ and $\mathbf{b}_0$ in Fig. 2 are in the forms

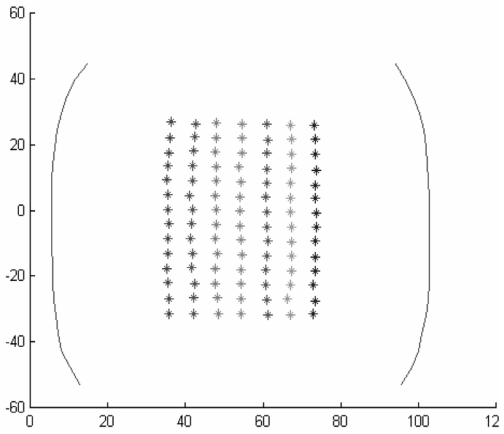

Fig. 3 Deformed shape and grid

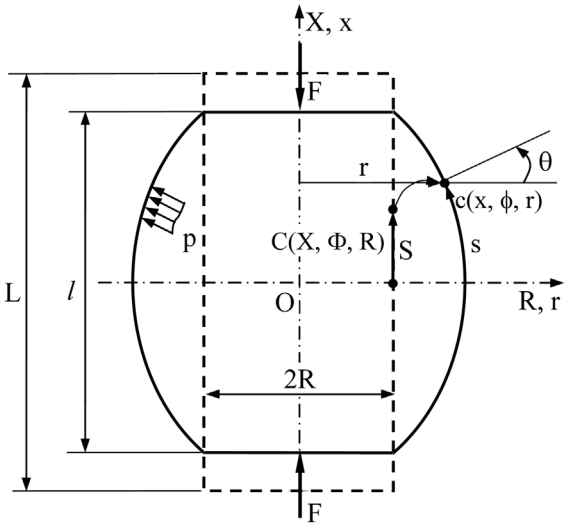

Fig. 4 Undeformed and deformed profiles of inflated cylindrical membrane

$$[\mathbf{a}_0] = [\cos\gamma \ \sin\gamma \ 0]^T, \quad [\mathbf{b}_0] = [\cos\gamma \ -\sin\gamma \ 0]^T \tag{1}$$

where γ is the (mean) angles between the fiber reinforced (arranged in symmetrical spirals) and the circumferential direction in the medium layer.

The experimental tests were carried out at five different positions of the air-spring. First the mounting plates of the non-loaded air-spring were fixed at the distance by 15, 20, 30, 40 or 50 mm shorter than the free height of the air-spring. Then the air-spring was loaded and unloaded gradually by pressurized air step 0.05 MPa in the range 0.1-0.5 MPa. Photographs of the deformed sheet were recorded by digital camera; the axial force and the inner pressure were measured and stored at every stage of loading. Digital photographs were processed semi-automatically by means of the Matlab image processing toolbox.

The centroids of deformed grid spots were calculated and the coordinates of contour points of the deformed CAS were recorded. The result of such processing is presented at Fig. 3. The deformations of CAS are determined from the photographic records of the deformed grid of points drawn on the surface of CAS through digital image processing techniques.

3. Deformation of inflated CAS

The main geometric features of the inflated membrane in according with the derivation of the works (Guo 2001) are determined. The CAS at Fig. 4 has the initial radius of mid-surface R, and length L. Its initial wall thickness H is assumed to be uniform. The undeformed profile of thin shell is described by polar coordinate system, (X, Φ, R). The cylindrical thin shell is inflated by the internal pressure p.

The deformed cylindrical thin shell is referred to the polar coordinate system (x, ϕ, r). A material particle moves during the deformation from the position in the undeformed profile, $C(X, \Phi, R)$ to

the deformed profile, $c(x, \phi, r)$, along its quasi-equilibrium path. Assume that the deformation is axisymmetric, then $\phi \equiv \Phi$. The principal stretch in axial and circumferential directions, principal curvatures and geometric relations are

$$\lambda_1 = \frac{ds}{dS}, \quad \lambda_3 = \frac{r}{R}, \quad \frac{dr}{ds} = -\sin\theta, \quad \frac{dx}{ds} = \cos\theta, \quad \kappa_1 = \frac{d\theta}{ds}, \quad \kappa_2 = \frac{\cos\theta}{r} \tag{2}$$

where s is the arc length measured from pole ($x = 0$) to the particle c (x, ϕ, r) along the meridian of the deformed profile. S is the length corresponding to s in the undeformed profile. An auxiliary variable θ is introduced as the angle of the tangent line. The radius r and the thickness h of the membrane are with respect to the deformed configuration. The radial stretch λ_3 is determined from the incompressibility constraint

$$\lambda_1\lambda_2\lambda_3 = 1 \quad \text{then} \quad h = \frac{H}{\lambda_1\lambda_2} \tag{3}$$

4. An orthotropic hyperelastic constitutive model

The formulation of the anisotropic constitutive model has the main advantage that all involved material parameters may be associated with the material constituents, i.e., matrix materials and the fibers. The orthotropic hyperelastic materials in this paper are considered incompressible composite materials with two families of fibers. Let's assume the isochoric deformation and neglect the dissipation due to irreversible effects. The free energy of the orthotropic hyperelastic materials is considered stored in the matrix material and fibers. Thus, a proposed strain energy function is considered the combination of scalar-value functions corresponding to energy stored in matrix material and the fibers parts

$$\Psi = \Psi_{\text{iso}} + \Psi_{\text{aniso}} \tag{4}$$

where Ψ_{iso} is the component of strain energy function for isotropic properties of materials. Ψ_{aniso} is the component of strain energy function for anisotropic properties.

The isotropic component of strain energy function may be involved by the strain energy function of Ogden's model (Ogden 2001) as

$$\Psi_{\text{iso}} = \Psi_{\text{iso}}(\lambda_1, \lambda_2, \lambda_3) = \sum_{n=1}^{3} \frac{\mu_n}{\alpha_n}(\lambda_1^{\alpha_n} + \lambda_2^{\alpha_n} + \lambda_3^{\alpha_n} - 3) \tag{5}$$

where λ_1, λ_2, and λ_3 are the three principal stretches. The parameters μ_n and α_n ($n = 1 \div 3$) of Ogden's model of rubber (Holzapfel 2000) are

$$\mu_1 = 0.63 \text{ MPa}, \quad \mu_2 = 0.0012 \text{ MPa}, \quad \mu_3 = -0.01 \text{ MPa}, \quad \alpha_1 = 1.3, \quad \alpha_2 = 5, \quad \alpha_3 = -2$$

Suppose that the reinforcing fibers are double-helically arranged in the matrix material symmetrically to the circumferential direction then the component of strain energy function for anisotropic property is expressed in terms of principal stretches in the form of exponential function

$$\Psi_{\text{aniso}} = \frac{k_1}{k_2}\{\exp[k_2(\lambda_2^2\cos^2\gamma + \lambda_1^2\sin^2\gamma - 1)^2] - 1\} \tag{6}$$

where 2γ is the angle of the two families of reinforced fibers, k_1 is stress-like material parameter and k_2 is a dimensionless parameter (Holzapfel and Gasser 2001). They are determined from the experimental results and from the 2D cylindrical membrane approximation. The angle γ of fibers is supposed to be 48.8^o.

The strain energy function of rubber-textile cord composite of inflated air-spring shell in two dimensional problem with incompressibility constraint can be supposed in the form

$$\Psi(\lambda_1, \lambda_2) = \sum_{n=1}^{3}\frac{\mu_n}{\alpha_n}(\lambda_1^{\alpha_n} + \lambda_2^{\alpha_n} + \lambda_1^{-\alpha_n}\lambda_2^{-\alpha_n} - 3) + \frac{k_1}{k_2}\{\exp[k_2(\lambda_2^2\cos^2\gamma + \lambda_1^2\sin^2\gamma - 1)^2] - 1\} \tag{7}$$

In principle the parameters μ_n and α_n ($n = 1 \div 3$) of strain energy function must be determined from the experimental data. But the influence of matrix constituent of rubber-textile cord composites since applied load of inflation is unimportant, because rubber matrix only preserves the integrity of the composite and transfers the load. Furthermore the material parameter k_1 and k_2 of strain energy function in which k_2 is expressed in the form of exponential function are very important in computations of rubber-textile cord composites with high anisotropy, because the reinforced textile cords support most applied loads. On the other hand the determination of these parameters μ_n, α_n ($n = 1 \div 3$), k_1 and k_2 from experimental data is very complex. Therefore the parameters μ_n and α_n ($n = 1 \div 3$) of rubber-like model of Ogden are selected firstly in our study. The parameters k_1 and k_2 are determined from experimental results and may contain the influences to the final results for all constituents of rubber-textile cord composites.

5. Identification of material parameters

Constitutive equations are the stress-strain relationships for the deformed membrane. If the strain energy function Ψ is an invariant, we may regard Ψ as a function of the principal stretches λ_a ($a = 1, 2, 3$). The principal Cauchy stresses associated with this deformation are given from strain energy function (Holzapfel 2000)

$$\sigma_a = -p^* + \lambda_a\frac{\partial\Psi}{\partial\lambda_a}, \quad a = 1, 2, 3 \tag{8}$$

where p^* is the indeterminate Lagrange multiplier (hydrostatic pressure).

By regarding inflation two of the stretches as dependent and treating the strain energy as a function of these through the definition $\Psi(\lambda_1, \lambda_2)$, the constitutive equations are obtained

$$\begin{aligned}
\sigma_1 - \sigma_3 &= \lambda_1\frac{\partial\Psi(\lambda_1, \lambda_2)}{\partial\lambda_1} \\
\sigma_2 - \sigma_3 &= \lambda_2\frac{\partial\Psi(\lambda_1, \lambda_2)}{\partial\lambda_2} \\
\sigma_2 - \sigma_1 &= \lambda_2\frac{\partial\Psi(\lambda_1, \lambda_2)}{\partial\lambda_2} - \lambda_1\frac{\partial\Psi(\lambda_1, \lambda_2)}{\partial\lambda_1}
\end{aligned} \tag{9}$$

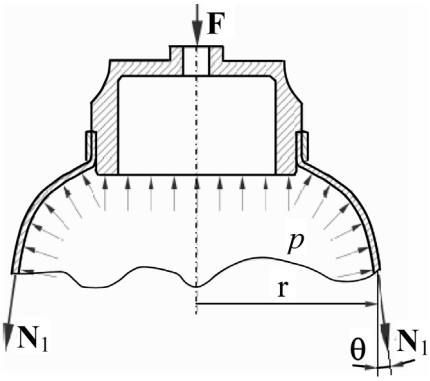

Fig. 5 Force equilibrium model of air-spring shell

The theory of nonlinear membranes has been presented by Green and Adkins (1965) and applied to various inflated structures (Guo 2001). The quasi-static equilibrium equations of problem are

$$\frac{d}{ds}(T_1 r) = T_2 \frac{dr}{ds} \tag{10}$$

$$\kappa_1 T_1 + \kappa_2 T_2 = p \tag{11}$$

where T_1 and T_2 are the stress resultant forces per unit length of the meridional and circumferential directions respectively. κ_1 and κ_2 are principal curvatures for the deformed membrane surface (2). Suppose that σ_1 and σ_2 are the principal Cauchy stresses at the particle. According to the assumptions for the membrane theory (Green and Adkins 1965), the stress resultant forces in the deformed configuration are

$$\begin{aligned} T_1 &= h(\sigma_1 - \sigma_3) \\ T_2 &= h(\sigma_2 - \sigma_3) \end{aligned} \tag{12}$$

The experimental series of the inflated cylindrical air-spring with the variable axial force F and the inner pressure p are effectuated. The Cauchy stress σ_1 is determined from the equilibrium in Fig. 5

$$N_1 \cos\theta = p\pi r^2 - F \Rightarrow \sigma_1 = \frac{p\pi r^2 - F}{2\pi r h \cos\theta} \tag{13}$$

By substituting $r = \lambda_2 R$ and $h = H/\lambda_1\lambda_2$ from (2) and (3) into (13) the stress is obtained as

$$\sigma_1 = A\frac{1}{\cos\theta}\lambda_1(\lambda_2^2 - B), \quad \text{in which} \quad A = \frac{pR}{2H}, \quad B = \frac{F}{\pi p R^2} \tag{14}$$

The stress σ_2 can be derived from equilibrium Eqs. (11) and (12). According to the theory of inflated membrane the stress σ_3 is assumed equal $-p$.

After the substitution of the Cauchy stresses into Eq. (9) a set of the nonlinear equations for the two variables k_1 and k_2 with the strain energy function presented in Eq. (7) is obtained as

$$\begin{cases} \sum_{n=1}^{3} \mu_n[\lambda_1^{\alpha_n} - (\lambda_1\lambda_2)^{-\alpha_n}] + 4k_1\exp(k_2m^2)m\lambda_1^2\sin^2\alpha = C + p \\ \sum_{n=1}^{3} \mu_n[\lambda_2^{\alpha_n} - (\lambda_1\lambda_2)^{-\alpha_n}] + 4k_1\exp(k_2m^2)m\lambda_2^2\cos^2\alpha = p(D+1) - C\frac{\kappa_1}{\kappa_2}\left(1 + \frac{\kappa_1}{\kappa_2}\right) \\ \sum_{n=1}^{3} \mu_n[\lambda_2^{\alpha_n} - \lambda_1^{\alpha_n}] + 4k_1\exp(k_2m^2)m(\lambda_2^2\cos^2\alpha - \lambda_1^2\sin^2\alpha) = pD - C \end{cases} \tag{15}$$

where $C = \frac{p}{2H\cos\theta}\frac{1}{\lambda_1}\left(\lambda_2^2R - \frac{F}{\pi Rp}\right)$, $D = \frac{pR}{H\cos\theta}\lambda_1\lambda_2^2$, $m = \lambda_2^2\cos^2\alpha + \lambda_1^2\sin^2\alpha - 1$.

The experimentally measured values of λ_1 and λ_2 in several points of the central part of the CAS were substituted into the Eq. (15). Taking the logarithm of (15) we will get a set of linear equations for the variables $\ln k_1$ and k_2. The resulting overdetermined system of linear equations was solved in Matlab. The result of parameters in our calculated program were $k_1 = 41.87$ MPa and $k_2 = -23.77$. The function of the Helmholtz energy potential for these parameters is convex.

6. Large deformation analysis by numerical integration

After the substitution of (2), (3), (8) and (12) into equilibrium equations of (10) and (11) and by some simplifications the system of five ordinary differential equations for the principal stretches λ_1 and λ_2, the tangent angle θ, the coordinate x in the deformed configuration and the inner pressure p with respect to the coordinate X of the undeformed configuration is obtained as

$$\begin{cases} \frac{d\lambda_1}{dX} = \frac{1}{\frac{A}{\cos\theta}(\lambda_2^2 - B) - M}\left[\frac{\lambda_1\sin\theta}{R}\left(N - A\frac{2}{\cos\theta}\lambda_1\lambda_2\right) + A\frac{\sin\theta}{\cos^2\theta}\lambda_1(\lambda_2^2 - B)Q\right] \\ \frac{d\lambda_2}{dX} = -\lambda_1R^{-1}\cdot\sin\theta, \quad \frac{d\theta}{dX} = Q, \quad \frac{dx}{dX} = \lambda_1\cdot\cos\theta, \quad \frac{dp}{dX} = 0 \end{cases} \tag{16}$$

where

$$Q = \frac{1}{R}\frac{\cos\theta}{A(\lambda_2^2 - B)}\left\{\frac{\cos\theta}{\lambda_2}\left[-p + \sum_{n=1}^{3} \mu_n[\lambda_2^{\alpha_n} - (\lambda_1\lambda_2)^{-\alpha_n}] + 4k_1\exp(k_2m^2)m\lambda_2^2\cos^2\alpha\right] - 2A\lambda_1\lambda_2\right\}$$

$$M = \frac{1}{\lambda_1}\sum_{n=1}^{3} \mu_n\alpha_n[\lambda_1^{\alpha_n} + (\lambda_1\lambda_2)^{-\alpha_n}] + 8k_1\exp(k_2m^2)\lambda_1\sin^2\alpha[\lambda_1^2\sin^2\alpha(2k_2m^2 + 1) + m]$$

$$N = \frac{1}{\lambda_2}\sum_{n=1}^{3} \mu_n\alpha_n(\lambda_1\lambda_2)^{-\alpha_n} + 8k_1\exp(k_2m^2)\lambda_1^2\lambda_2\sin^2\alpha\cos^2\alpha(2k_2m^2 + 1)$$

The set of differential Eq. (16) is solved by the shooting method in Matlab with the boundary condition for λ_1^0 and λ_2^0 determined from the experiments. The calculated deformed profiles and stretches of CAS are shown and compared with experimental ones in the following figures.

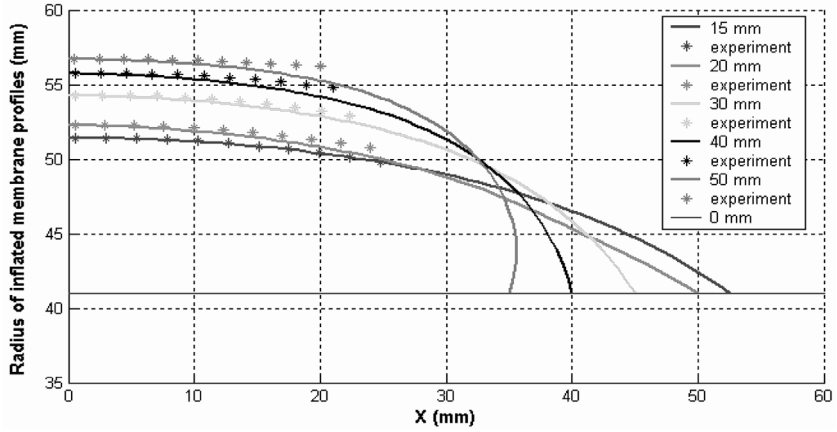

Fig. 6 The deformed profiles with shortening length 15, 20, 30, 40 and 50 mm under internal pressure p = 0.5 MPa

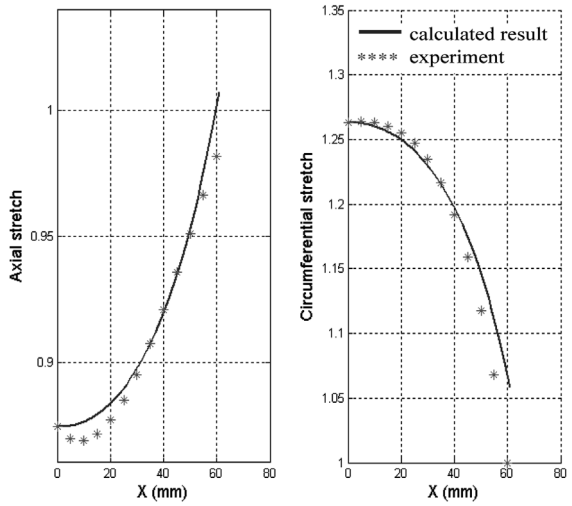

Fig. 7 The axial and circumferential stretches with shortening length 15 mm under internal pressure p = 0.4 MPa

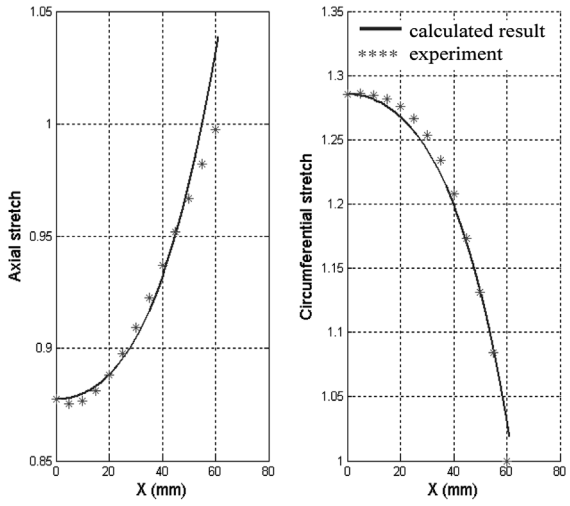

Fig. 8 The axial and circumferential stretches with shortening length 15 mm under internal pressure p = 0.5 MPa

Fig. 6 describes the deformed profiles of cylindrical shell of air-spring under internal pressure p = 0.5 MPa with shortening length 15, 20, 30, 40 and 50 mm. These results show that the deformation of material is large. The deformed profiles along the length of cylindrical shell subjected to different internal pressure are calculated and respond well to experimental results.

Fig. 7 and Fig. 8 describe the axial and circumferential stretches with shortening length 15 mm under internal pressure p = 0.4 MPa and 0.5 MPa. The axial stretches in the cylindrical shell are less than 1 (shortening of the shell due to the inflation) and the circumferential stretches are greater than 1. The numerical results show that the presented constitutive material model is appropriate for the deformation analysis of the CAS made from the given composite material.

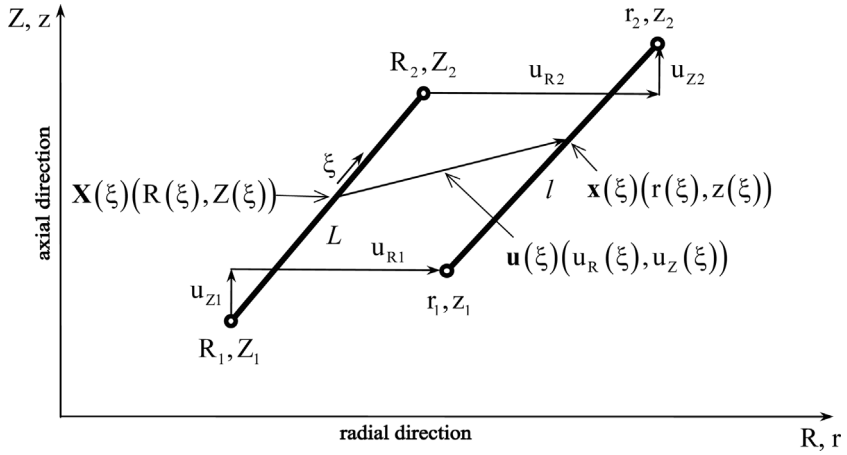

Fig. 9 An axisymmetric shell element

7. Large deformation analysis by FEM

7.1 Basic equations of nonlinear finite element formulation

7.1.1 The axisymmetric shell element

The axisymmetric shell element that has length of L and thickness of H in the reference configuration and length of l in the current configuration is presented in Fig. 9. This element has two nodes and the vector of node displacement is $\mathbf{u}$.

The coordinates in reference and current configuration and displacement vector are interpolated linearly as the functions of the isoparametric coordinate ξ

$$\mathbf{X}(\xi) = \mathbf{N} \cdot \{R_1, Z_1, R_2, Z_2\}^T, \quad \mathbf{x}(\xi) = \mathbf{N} \cdot \{r_1, z_1, r_2, z_2\}^T \tag{17}$$

$$\mathbf{u}(\xi) = \mathbf{x}(\xi) - \mathbf{X}(\xi) = \mathbf{N} \cdot \mathbf{u}, \quad \mathbf{u} = \{u_{R1}, u_{Z1}, u_{R2}, u_{Z2}\}^T \tag{18}$$

where $\mathbf{N}$ is the matrix of shape functions

$$\mathbf{N} = \begin{bmatrix} \mathbf{N}_1 \\ \mathbf{N}_2 \end{bmatrix} = \frac{1}{2}\begin{bmatrix} 1-\xi & 0 & 1+\xi & 0 \\ 0 & 1-\xi & 0 & 1+\xi \end{bmatrix} \tag{19}$$

Green-Lagrange deformation tensor (GL) and second Piola-Kirchhoff strain tensor (PK2) are used as the conjugate pair in order to express the strain energy in the Lagrangian description.

The axial Green strain can be found from the change of length element (Shi and Moita 1996)

$$E_{11} = \frac{l^2 - L^2}{2L^2} = [\mathbf{b}_{1l} + \mathbf{b}_{1n}(\mathbf{u})] \cdot \mathbf{u} \tag{20}$$

where $\begin{cases} \mathbf{b}_{1l} = \dfrac{1}{L^2}\{R_1, Z_1, R_2, Z_2\} \cdot \mathbf{A} \\ \mathbf{b}_{1n}(\mathbf{u}) = \dfrac{1}{2L^2}\mathbf{u}^T \cdot \mathbf{A} \end{cases}$ with $\mathbf{A} = \begin{bmatrix} 1 & 0 & -1 & 0 \\ 0 & 1 & 0 & -1 \\ -1 & 0 & 1 & 0 \\ 0 & -1 & 0 & 1 \end{bmatrix}$

The hoop component of GL is determined from the change of the circumferential length

$$E_{22} = \frac{\mathbf{o}^2 - \mathbf{O}^2}{2\mathbf{O}^2} = \frac{u_R(\xi)}{R(\xi)} + \frac{1}{2}\left(\frac{u_R(\xi)}{R(\xi)}\right)^2 = e_l + \frac{1}{2}e_l^2; \quad e_l = \frac{1}{R(\xi)}\mathbf{N}_1 \cdot \mathbf{u} \tag{21}$$

The variation $\delta\mathbf{E}$ can be expressed by variation $\delta\mathbf{u}$ in the following form

$$\delta\mathbf{E} = \begin{Bmatrix} \delta E_{11} \\ \delta E_{22} \end{Bmatrix} = \mathbf{B}_{nl} \cdot \delta\mathbf{u} \tag{22}$$

where $\mathbf{B}_{nl} = \begin{bmatrix} \mathbf{B}_{nl1} \\ \mathbf{B}_{nl2} \end{bmatrix} = \begin{bmatrix} \dfrac{1}{L^2}\left(\{R_1, Z_1, R_2, Z_2\} + \dfrac{1}{2}\mathbf{u}^T\right) \cdot \mathbf{A} \\ \left(1 + \dfrac{1}{2R(\xi)}\mathbf{N}_1 \cdot \mathbf{u}\right)\dfrac{1}{R(\xi)}\mathbf{N}_1 \end{bmatrix}$

The components of PK2 can be deduced from strain energy function according to the relation

$$S_{ii} = \frac{1}{\lambda_i}\frac{\partial\Psi}{\partial\lambda_i}, \quad i = 1, 2 \tag{23}$$

where $\begin{cases} S_{11} = \displaystyle\sum_{a=1}^{3}\frac{\mu_a}{\lambda_1^2}[\lambda_1^{\alpha_a} - (\lambda_1\lambda_2)^{-\alpha_a}] + 4k_1 m\exp(k_2 m^2)\sin^2\gamma \\ S_{22} = \displaystyle\sum_{a=1}^{3}\frac{\mu_a}{\lambda_2^2}[\lambda_2^{\alpha_a} - (\lambda_1\lambda_2)^{-\alpha_a}] + 4k_1 m\exp(k_2 m^2)\cos^2\gamma \end{cases}$ (24)

Furthermore, the components E_{11} a E_{22} of GL can be obtained in the term of principal stretches as

$$E_{ii} = \frac{\lambda_i^2 - 1}{2} \Rightarrow \frac{\partial\lambda_i}{\partial E_{ii}} = \frac{1}{\lambda_i}, \quad i = 1, 2 \tag{25}$$

The elastic tensor $\mathbb{C}$ is determined from principal components of PK2

$$\mathbb{C} = \frac{\partial\mathbf{S}}{\partial\mathbf{E}}, \quad \mathbb{C} = \begin{bmatrix} \dfrac{1}{\lambda_1}\dfrac{\partial S_{11}}{\partial\lambda_1} & \dfrac{1}{\lambda_2}\dfrac{\partial S_{11}}{\partial\lambda_2} \\ \dfrac{1}{\lambda_1}\dfrac{\partial S_{22}}{\partial\lambda_1} & \dfrac{1}{\lambda_2}\dfrac{\partial S_{22}}{\partial\lambda_2} \end{bmatrix}, \quad \mathbf{S} = \mathbb{C}\mathbf{E} \tag{26}$$

$$\mathbb{C}_{11} = \frac{1}{\lambda_1^4}\sum_{a=1}^{3}\mu_a[(\alpha_a - 2)\lambda_1^{\alpha_a} + (\alpha_a + 2)(\lambda_1\lambda_2)^{-\alpha_a}] + 8k_1\exp(k_2 m^2)\sin^4\gamma(1 + 2k_2 m^2)$$

$$\mathbb{C}_{12} = \mathbb{C}_{21} = \frac{1}{\lambda_1^2\lambda_2^2}\sum_{a=1}^{3}\mu_a\alpha_a(\lambda_1\lambda_2)^{-\alpha_a} + 8k_1\exp(k_2m^2)\sin^2\gamma\cos^2\gamma(1+2k_2m^2)$$

$$\mathbb{C}_{22} = \frac{1}{\lambda_2^4}\sum_{a=1}^{3}\mu_a[(\alpha_a-2)\lambda_2^{\alpha_a} + (\alpha_a+2)(\lambda_1\lambda_2)^{-\alpha_a}] + 8k_1\exp(k_2m^2)\cos^4\gamma(1+2k_2m^2)$$

Note that the elasticity tensor is not constant, but depends on the deformations and then must be updated in every iterative step.

7.1.2 Principle of virtual work and its linearization

Principle of virtual work in given problem can be written in the following form:

$$R(\mathbf{u}, \delta\mathbf{u}, p) = \int_{\Omega_0}\mathbf{S}:\delta\mathbf{E}dV - p\int_{\partial\Omega}\mathbf{n}^T\cdot\delta\mathbf{u}ds \equiv 0 \tag{27}$$

in which p is the internal pressure, $\delta\mathbf{u}$ stands for a virtual displacement vector, Ω_0 is undeformed volume, $\partial\Omega$ represents the deformed shell surface and $\mathbf{n}$ is the normal vector of deformed shell surface.

The principle of virtual work can be expressed through introduction of the external load factor λ as

$$R(\mathbf{u}, \delta\mathbf{u}, \lambda) = \mathbf{R}(\mathbf{u}, \lambda)^T\cdot\delta\mathbf{u} = (\mathbf{f}_{\text{int}}(\mathbf{u}) - \lambda\mathbf{f}_{\text{ext}}(\mathbf{u}))^T\cdot\delta\mathbf{u} \tag{28}$$

In this equation $\mathbf{u}$ is the nodal displacement vector (18), $\mathbf{R}(\mathbf{u}, \lambda)$ represents the out-of-balance force which must be equal to zero to ensure equilibrium. Moreover $\mathbf{R}(\mathbf{u}, \lambda)$ can be written under the following form

$$\mathbf{R}(\mathbf{u}, \lambda) = \mathbf{f}_{\text{int}}(\mathbf{u}) - \lambda\mathbf{f}_{\text{ext}}(\mathbf{u}) \tag{29}$$

The internal force vector of element can be introduced from the first integral of principle of virtual work (27) by replacing $\delta\mathbf{E}$ from (22) and $dV = 2\pi R(\xi)HLd\xi$

$$\mathbf{f}_{\text{int}}^{\ e} = \int_{-1}^{1}\mathbf{B}_{nl}^T\mathbf{S}2\pi R(\xi)HLd\xi \tag{30}$$

Similarly the external force vector of element can be introduced from the second integral of principle of virtual work (27) by replacing $ds = 2\pi R(\xi)ld\xi$

$$\mathbf{f}_{\text{ext}}^{\ e} = \int_{-1}^{1}\mathbf{N}^T\cdot\mathbf{n}(\xi)2\pi r(\xi)ld\xi \tag{31}$$

where $\mathbf{n}(\xi) = \frac{1}{l}\begin{Bmatrix} z_2 - z_1 \\ -(r_2 - r_1)\end{Bmatrix}$, $r(\xi) = \mathbf{N}_1\cdot\{r_1, z_1, r_2, z_2\}^T$

Now a system of nonlinear equation is obtained in the following form

$$\mathbf{f}_{\text{int}}(\mathbf{u}) - \lambda\mathbf{f}_{\text{ext}}(\mathbf{u}) = \mathbf{0} \tag{32}$$

In order to solve the nonlinear Eq. (32), the classical tangent stiffness matrix $\mathbf{K}_t = \frac{\partial \mathbf{R}(\mathbf{u}, \lambda)}{\partial \mathbf{u}} = [\mathbf{K}_{int} - \mathbf{K}_{ext}]$ has to be defined (Chevaugeon *et al.* 2002). The stiffness matrix $\mathbf{K}_t$ is expressed in the following form

$$\mathbf{K}_t = \left[\frac{\partial \mathbf{f}_{int}}{\partial \mathbf{u}} - \lambda \frac{\partial \mathbf{f}_{ext}}{\partial \mathbf{u}}\right] \tag{33}$$

By the derivation of internal force vector (30) with respect to the displacements, it follows that

$$\frac{\partial \mathbf{f}_{int}^{e}}{\partial \mathbf{u}} = \mathbf{K}_M^e + \mathbf{K}_G^e \tag{34}$$

$$\mathbf{K}_M^e = \int_{-1}^{1} \mathbf{B}_{nl}^T \mathbb{C}\, \mathbf{B}_{nl} 2\pi R(\xi) HL d\xi$$

$$\mathbf{K}_G^e = \int_{-1}^{1} \left(\frac{S_{11}}{2L^2}\mathbf{A} + \frac{S_{22}}{R^2(\xi)}\mathbf{N}_1^T \mathbf{N}_1\right) 2\pi R(\xi) HL d\xi$$

in which $\mathbf{K}_M^e$ is the standard stiffness matrix or initial displacement matrix and $\mathbf{K}_G^e$ is the geometric or initial stress stiffness matrix.

Similarly by the derivation of external force vector (31) with respect to the displacements will be obtained the following matrix

$$\mathbf{K}_p^e = \frac{\partial \mathbf{f}_{ext}^{e}}{\partial \mathbf{u}} = \frac{2\pi}{3}\begin{bmatrix} 2z_{21} & -(2r_1 + r_2) & z_{21} & 2r_1 + r_2 \\ 4r_1 - r_2 & 0 & -(r_1 + 2r_2) & 0 \\ z_{21} & -(r_1 + 2r_2) & 2z_{21} & r_1 + 2r_2 \\ 2r_1 + r_2 & 0 & r_1 - 4r_2 & 0 \end{bmatrix} \tag{35}$$

$$z_{21} = z_2 - z_2, \{r_1, z_1, r_2, z_2\} = \{R_1, Z_1, R_2, Z_2\} + \{u_{R1}, u_{Z1}, u_{R2}, u_{Z2}\}$$

The total stiffness matrix for one element is determined by the initial displacement matrix $\mathbf{K}_M^e$, the initial stress matrix $\mathbf{K}_G^e$ and the crucial load tangent stiffness matrix caused deformation dependent loads (Holzapfel *et al.* 1996), as:

$$\mathbf{K}_t^e = \mathbf{K}_M^e + \mathbf{K}_G^e - \lambda^e \mathbf{K}_p^e \tag{36}$$

7.2 Nonlinear numerical solution

The basic approach to solve the nonlinear responses is the incremental-iterative method or the continuation method, also called path-following method determining the equilibrium points on the load (pressure)-displacement paths or equilibrium paths. The incremental-iterative approach described here is based on a combination of the modified Newton-Raphson iterative method and the arc-length method. The tangent stiffness matrix and internal force vector and external force vector are updated not only at the commencement of every iterative cycle, but also at each load step (Fig. 10).

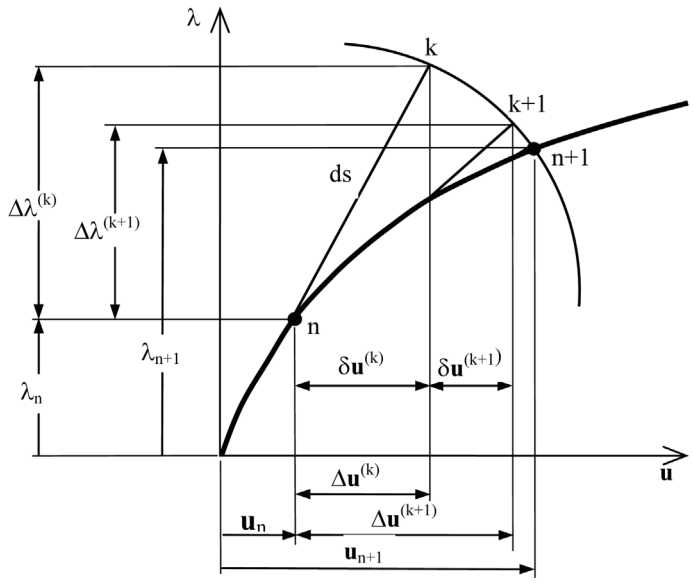

Fig. 10 The combination of modified Newton-Raphson and arc-length method

7.2.1 Predictor and corrector solutions

Consider a particular equilibrium point at an instant t_n on the equilibrium path which is defined by the nodal displacement $\mathbf{u}_n$ and load factor λ_n. The purpose of the numerical solution is to find one new equilibrium point on the path. The new point at subsequent instant t_{n+1} is defined by displacement and load factor increments denoted $\Delta\mathbf{u}$ and $\Delta\lambda$, respectively, and it satisfies simultaneously the following equations

$$\begin{cases} \mathbf{R}(\mathbf{u}_n + \Delta\mathbf{u}, \lambda_n + \Delta\lambda) = 0 \\ F(\Delta\mathbf{u}, \Delta\lambda) = 0 \end{cases} \tag{37}$$

The first equation is the residual equation and the second one is extra equation which is normally called arc-length constraint associated with path-following procedures. For the more widely used cylindrical arc-length method, the constraint equation is given in the following form (Crisfield 1997, De Souza Neto and Feng 1999)

$$\Delta\mathbf{u}^T\Delta\mathbf{u} = ds^2 \tag{38}$$

where ds is arc-length which is the control parameter.

Here the Newton-Raphson iterative method is now examined for solving the previous system (37). Consider the algorithm at a given iteration, the system to be solved is

$$\begin{cases} \mathbf{R}^{(k+1)} = \mathbf{R}^{(k)} + \dfrac{\partial\mathbf{R}}{\partial\Delta\mathbf{u}}\delta\mathbf{u} + \dfrac{\partial\mathbf{R}}{\partial\Delta\lambda}\delta\lambda = 0 \\ F^{(k+1)} = F^{(k)} + \dfrac{\partial\mathrm{A}}{\partial\Delta\mathbf{u}}\delta\mathbf{u} + \dfrac{\partial\mathrm{A}}{\partial\Delta\lambda}\delta\lambda = 0 \end{cases} \tag{39}$$

where subscripts $k+1$ and k, respectively, are for the current iteration and for the previous iteration. To solve (39) the displacement vector and incremental displacement are obtained as

$$\mathbf{u}_{n+1}^{(k+1)} = \mathbf{u}_n + \Delta\mathbf{u}^{(k+1)} \tag{40}$$

$$\Delta\mathbf{u}^{(k+1)} = \Delta\mathbf{u}^{(k)} + \delta\mathbf{u}^{(k+1)} \tag{41}$$

where $\Delta\mathbf{u}^{(k)}$ and $\Delta\mathbf{u}^{(k+1)}$ are the incremental displacement guesses for the previous and current iteration, respectively, and $\delta\mathbf{u}$ is the iteractive displacement. The incremental load factor, $\Delta\lambda$, is updated according to

$$\Delta\lambda^{(k+1)} = \Delta\lambda^{(k)} + \delta\lambda \tag{42}$$

Using the previous definition of the tangent stiffness matrix (33) the system (39) becomes

$$\begin{cases} \mathbf{R}^{(k+1)} = \mathbf{R}^{(k)} + \mathbf{K}_t(\mathbf{u}^{(k)})\delta\mathbf{u} - \delta\lambda\mathbf{f}_{\text{ext}}(\mathbf{u}^{(k)}) = 0 \\ F^{(k+1)} = F^{(k)} + 2\Delta\mathbf{u}^{(k)} \cdot \delta\mathbf{u} = 0 \end{cases} \tag{43}$$

The system of nonlinear equations for iterative solutions $\delta\mathbf{u}$ and $\delta\lambda$ (the corrector solution) is derived by simply linearising the residual equation and cylindrical arc-length equation using Taylor series. The system of Eq. (43) is written as

$$\begin{bmatrix} \mathbf{K}_t(\mathbf{u}^{(k)}) & -\mathbf{f}_{\text{ext}}(\mathbf{u}^{(k)}) \\ 2\Delta\mathbf{u}^{(k)T} & 0 \end{bmatrix} \begin{Bmatrix} \delta\mathbf{u} \\ \delta\lambda \end{Bmatrix} = -\begin{Bmatrix} R(\mathbf{u}^{(k)}, \Delta\lambda^{(k)}) \\ \Delta\mathbf{u}^T\Delta\mathbf{u} - ds^2 \end{Bmatrix} \tag{44}$$

where the subscript $n+1$ have been abandoned for notational convenience.

When $k=0$ (the predictor solution), the forward-Euler tangential predictor solution is adopted (Verron and Marckmann 2001). The two predicted increments $\Delta\bar{\mathbf{u}}$ and $\Delta\bar{\lambda}$ are supposed to satisfy the first equilibrium equation of (43) with $\mathbf{R}^{(0)} = 0$

$$\Delta\bar{\mathbf{u}} = \Delta\bar{\lambda}\,\delta\bar{\mathbf{u}} \tag{45}$$

where tangent displacement vector $\delta\bar{\mathbf{u}}$ is given by

$$\delta\bar{\mathbf{u}} = \mathbf{K}_t^{-1}\mathbf{f}_{\text{ext}} \tag{46}$$

The possible iteractive load factor $\delta\lambda$ for the predictor solution is

$$\delta\lambda = \pm\frac{ds}{\sqrt{\delta\bar{\mathbf{u}}^T\delta\bar{\mathbf{u}}}} \tag{47}$$

and the success of the path-following technique depends crucially on the choice of the appropriate sign for iterative load factor.

In order to predict the continuation direction, the sign of predictor load factor must be chosen. From the criterion of Feng *et al.* (1996) the sign of the predictor load factor is made to coincide

with the sign of the internal product between the previous converged incremental displacement $\Delta\mathbf{u}_n$, and the current tangential solution $\delta\overline{\mathbf{u}}$

$$\text{sign}(\delta\lambda) = \text{sign}(\Delta\mathbf{u}_n^T \delta\overline{\mathbf{u}}) \tag{48}$$

7.2.2 Step-length control

For controlling the step length size the arc-length for use in the current increment $(n+1)$ can be computed using the arc-length of previous increment (n) by

$$ds_{n+1} = ds_n \left(\frac{J_d}{J_n}\right)^{\eta} \tag{49}$$

in which ds_n is arc-length for previous load step n, J_n is actual number of iterations required for convergence in the previous load step, J_d is a user-defined desired number of iterations for convergence, typically 3 to 5. The exponent η usually lies in the range 0.5 to 1.0.

7.2.3 Convergence criteria

A some convergence criterion based on the incremental displacements or energy are presented (Clarke and Hancock 1990). The residual convergence criteria is introduced here. The Euclidean norm of residual is compared with some predefined tolerance:

$$\|\mathbf{R}(\mathbf{u}, \lambda)\| \leq \varepsilon_r \tag{50}$$

where typically ε_r is in the range 10^{-2} to 10^{-5}, depending on the desired accuracy and the non-linear charateristics of the particular problem.

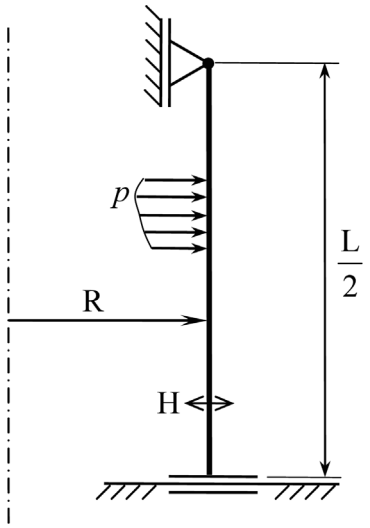

Fig. 11 FEM model of inflated cylindrical shell with free heads

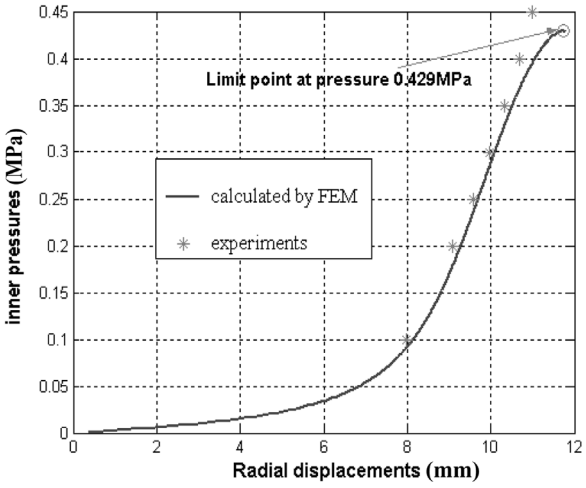

Fig. 12 Equilibrium paths in the case of free heads

7.3 Numerical results

In this section the inflation of a cylindrical CRC membrane of CAS is examined. The problem 2D geometry and the boundary condition are shown in Fig. 11. The material of air-spring is considerred the orthotropic hyperelastic material and modelled by constitutive equations through the strain energy function (7). The material parameters which were determined previously are used in FEM computation. Because of symmetrical distribution the half of CAS was discretized by 60 elements. In the first phase the calculation was implemented by selecting small incremental force and in every iterative step the iterations were performed until achievement the required tolerance. The combination of modified Newton-Raphson method and arc-length procedure was used in the next phase in which the stiffness matrix, internal and external force vector were updated not only in the beginning of every loading step, but also in every iterative cycle (Fig. 10).

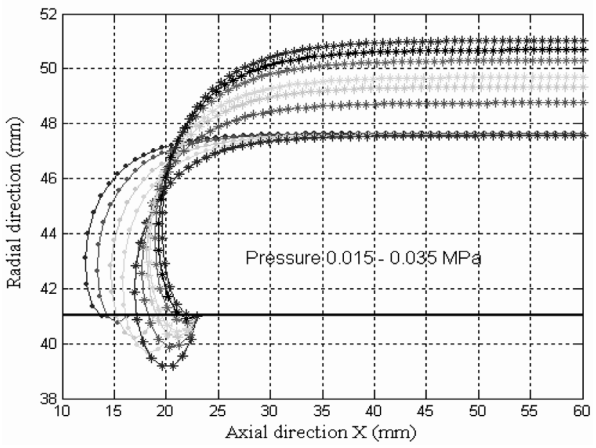

Fig. 13 Profiles of deformed shell at different stages of loading

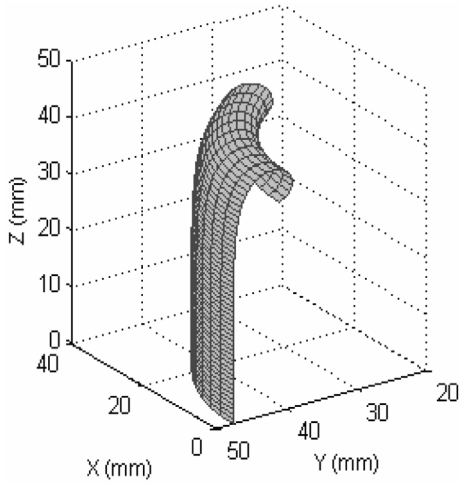

Fig. 14 Deformed shape under internal pressure p = 0.015 MPa

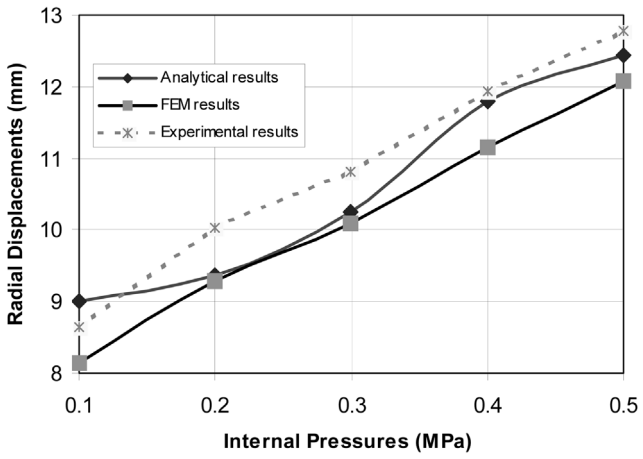

Fig. 15 The comparison between analytical, FEM and experimental results

Numerical results are obtained after simulation for the inflation of cylindrical shell by predictor-corrector method using our program script files written in Matlab. Fig. 12 describes equilibrium path between radial displacement with internal pressure. The equilibrium path is obtained up to overcome the limit point and corresponds with the experimental responses.

The profiles of deformed shell at different stages of loading are described in Fig. 13. Firstly the air-spring was loaded by pressurized air 0.015 MPa with free head of air-spring. Then the mounting plates of air-spring were fixed meanwhile the internal pressure comes up to 0.035 MPa. Fig. 14 describes the deformed shape of the CAS. Fig. 13 and Fig. 14 show that the ends of examined air-spring influence greatly its deformation. While these results are difficult to be determined by experiment.

Finally, the analytical results and FEM's results are compared with experimental ones in Fig. 15. It is seen that the radial displacements are in good agreement with the experimental ones. Maximal error for radial displacements between FE and experimental results is 6,5%. Therefore the presented constitutive model is suitable for study of mechanical behavior of the thin-walled CAS made of RCC.

The examined air-spring is relatively short and the ends influence greatly its deformation. It is evident from the presented figures once the heads of the air-spring approach together the deformed shapes become curved broadly near the heads of air-spring. These curved parts cannot be measured directly experimentally as they are not visible at recorded photographs. Thus the difference at these points between the estimated reality and the numerical simulation is not alarming. Whereas the accordance of numerically simulated and experimentally measured stretches and shapes is satisfactory in the central portion of the air-spring.

8. Conclusions

This study was conducted in respect of the mechanical response of a thin-walled cylindrical shell of air-spring under combined inflation and axial force with reference to fundamental continuum mechanical principles. The identification of the material parameters was solved through experimental results. The presented strain energy function was implemented into the calculus of deformations of the inflated CAS. The deformations were determined by numerical solution of the system of ordinary differential equations based on the membrane theory.

The nonlinear FE formulation for the finite strain behaviour has been derived and verified. The strain energy function (7) was used to set up the constitutive relations in the finite element analysis using Matlab code. Axisymmetric finite elements for the hyperelastic orthotropic material model were made up to simulate the deformation of an inflated cylindrical membrane. The highly nonlinear numerical procedure was mastered. Limit points were detected in the equilibrium following path by using combination of modified Newton-Raphson and arc-length methods in FE analysis. The developed finite elements are efficient and, in general, applicable for various materials in the large strain range. The performance of the both developed software and the accuracy of the numerical results have been demonstrated for several examples in which obtained numerical results answered to experimental responses.

Acknowledgements

This publication is completed with financial support from Vietnam Basic Research Program in Natural Science.

References

Beatty, M.F. (1987), "Topics in finite elasticity: Hyperelasticity of rubber, elastomers, and biological tissues with examples", *Appl. Mech. Rev.*, **40**(12), 1699-1734.

Bonet, J. and Burton, A.J. (1998), "A simple orthotropic, transversely isotropic hyperelastic constitutive equation for large strain computations", *Comput. Meth. Appl. Mech. Eng.*, **162**, 151-164.

Bonet, J. and Profit, M.L. (2000), "Nonlinear viscoelastic constitutive modeling of a continuum", *European Congress on Comput. Meth. Appl. Mech. Eng.,* Barcelona, 11-14 September.

Chevaugeon, N., Marckmann, G., Verron, E. and Peseux, B. (2002), "Instabilité et bifurcation du souffage de membranes hyperélastiques", *REEF*, 479-492.

Clarke, M.J. and Hancock, G.J. (1990), "A study of incremental-iterative strategies for nonlinear analyses", *Int. J. Numer. Meth. Eng.*, **29**, 1365-1391.

De Souza Neto, E.A. and Feng, Y.T. (1999), "On the determination of the path direction for arc-length methods in the presence of bifurcations and 'snap-backs'", *Comput. Meth. Appl. Mech. Eng.*, **179**, 81-89.

Feng, Y.T., Peric, D. and Owen, D.R.J. (1996), "A new criterion for determination of initial loading parameter in arc-length methods", *Comput. Struct.,* **58** (3), 479-485.

Green, A.E. and Adkins, J.E. (1965), "Bolšije uprugie deformaci i nelinejnaja mechanika splošnoj stredy", Moskva.

Guo, X. (2001), "Large deformation analysis for a cylindrical hyperelastic membrane of rubber-like material under internal pressure", *Rubber Chemistry and Technology*, **74**, 100-115.

Holzapfel, G.A., Eberlein, R., Wriggers, P. and Weizsacker, H.W. (1996), "Large strain analysis of soft biological membranes: Formulation and finite element analysis", *Comput. Meth. Appl. Mech. Eng.*, **132**, 45-61.

Holzapfel, G.A., Gasser, T.C. and Ogden, R.W. (2000), "A new constitutive framework for arterial wall mechanics and a comparative study of material models", *J. of Elasticity*, **61**, 1-48.

Holzapfel, G.A. and Gasser, T.C. (2001), "A viscoelastic model for fiber-reinforced composites at finite strains: Continuum basis, computational aspects and applications", *Comput. Meth. Appl. Mech. Eng.,* **190**, 4379-4430.

Holzapfel, G.A. (2000), *Nonlinear Solid Mechanics*, John Wiley & Sons Ltd, ISBN: 0-471-82319-8, Chichester West Sussex PO19, England.

Jiang, L. and Haddow, J.B. (1995), "A finite element formulation for finite static axisymmetric deformation of hyperelastic membranes", *Comput. Struct.,* **57**, 401-405.

Ogden, R.W. (2001), "Background on nonlinear elasticity", Lemaitre J., ed., in the *Handbook of Materials Behavior Models*, Chapter 2.2, Academic Press, Boston, 75-83.

Ogden, R.W. and Schulze-Bauer, C.A.J. (2000), "Phenomenological and structural aspects of the mechanical response of arteries", appeared as *Proc. in Mechanics in Biology*, J. Casey and G. Bao, eds., AMD-242, BED-**46**, New York, 125-140.

Poživilová, A. and Plešek, J. (2002), "Elastomery: Konstitutivní modelování, identifikace materiálových parametrů a porovnání s experimentem", *Inženýrká mechanika*, Svratka, Česká Republika.

Reese, S. (2000), "Large deformation FE modeling of the orthotropic elastoplastic material behavior in pneumatic membranes", *European Congress on Comput. Methods Appl. Mech. Eng.,* Barcelona, 11-14 September.

Reese, S., Raible, T. and Wriggers, P. (2001), "Finite element modeling of orthotropic material behavior in pneumatic membranes", *Int. J. Solids Struct.*, **38**, 9525-9544.

Shi, J. and Moita, G.F. (1996), "The post-critical analysis of axisymmetric hyper-elastic membranes by finite element method", *Comput. Meth. Appl. Mech. Eng.*, **135**, 265-281.

Verron, E. and Marckmann, G. (2001), "An axisymmetric B-spline model for the non-linear inflation of

rubberlike membranes", *Comput. Meth. Appl. Mech. Eng.*, **190**, 6271-6289.
Verron, E. and Marckmann, G. (2003), "Inflation of elastomeric circular membranes using network constitutive equations", *Int. J. of Non-Linear Mechanics*, **38**, 1221-1235.
Wriggers, P. and Taylor, R.L. (1990), "A fully non-linear axisymmetrical membrane element for rubber-like materials", *Eng. Comput.*, **7**, 303-310.